Strong Angular-Momentum Optomechanical Coupling for Macroscopic Quantum Control

Yuan Liu,[1,2] Yaoming Chu,[1,2] Shaoliang Zhang,[1,2,*] and Jianming Cai[1,2,†]

[1] *School of Physics, Hubei Key Laboratory of Gravitation and Quantum Physics, Institute for Quantum Science and Engineering, International Joint Laboratory on Quantum Sensing and Quantum Metrology, Huazhong University of Science and Technology, Wuhan 430074, China*

[2] *Wuhan National Laboratory for Optoelectronics, Huazhong University of Science and Technology, Wuhan 430074, China*

(Received 21 September 2021; revised 15 April 2022; accepted 18 April 2022; published 11 May 2022; corrected 18 July 2022)

Optomechanical systems offer unique opportunities to explore macroscopic quantum state and related fundamental problems in quantum mechanics. Here, we propose a quantum optomechanical system involving exchange interaction between spin angular momentum of light and a torsional oscillator. We demonstrate that this system allows coherent control of the torsional quantum state of a torsional oscillator on the single-photon level, which facilitates efficient cooling and squeezing of the torsional oscillator. Furthermore, the torsional oscillator with a macroscopic length scale can be prepared in Schrödinger catlike state. Our work provides a platform to verify the validity of quantum mechanics in macroscopic systems on the micrometer and even centimeter scale.

DOI: 10.1103/PhysRevApplied.17.054017

I. INTRODUCTION

Optomechanics has attracted considerable focus recently, ranging from applied science in high-sensitivity metrology [1–3] and quantum-information processes [4–7] to basic science, such as the ground-state cooling of a mechanical oscillator [8], squeezing of both the optical [9,10] as well as the mechanical mode [11,12], and quantum entanglement at macroscopic scale [13–15]. However, in almost all of the optomechanical systems mentioned above, the optomechanical interaction between light and matter is induced by the linear momentum exchange interaction.

It is well known that in addition to exchange linear momentum with matter, light can also exchange angular momentum with matter [16–21]. This opens the door to different possibilities in the engineering of an optomechanical system. For example, the angular momentum of light may provide an effective way to manipulate the rotational quantum state of a spiral phase plate [22], and to drive the rotational degree of other mechanical oscillators, such as levitated nanoparticles [23–25] and integrated optical waveguides [26,27]. These angular momentum optomechanical systems not only enable people to detect torque with ultrahigh sensitivity [23–25] and provide a different paradigm for detecting the van der Waals and Casimir torque [28–30], measuring vacuum friction [31,32], but also can be utilized in quantum-information processes, such as optomechanical entanglement between torsional mode phonon and cavity photon [33], etc. Despite these exciting developments, the challenge remains in achieving strong angular-momentum optomechanical interaction between light and torsional oscillators with macroscopic length scale [23–27], which would lead to interesting macroscopic quantum phenomena and extend the research scope of quantum optomechanics.

In this paper, we theoretically propose an optomechanical system with strong exchange interaction between spin angular momentum of light and a long (length $L \approx 0.1\ \mathrm{mm} - 1\ \mathrm{cm}$) torsional oscillator of optical anisotropy and demonstrate the effective cooling, squeezing, and Schrödinger catlike state [34] preparation of the torsional degree of freedom of the torsional oscillator. The torsional motion of the optical anisotropic torsional oscillator destroys the diagonality of the permittivity tensor of our optomechanical resonator, and thus induces strong cross-optomechanical interaction between two orthogonal optical modes and the torsional motion mode. Besides, the usage of an integrated photonic device in our optomechanical system effectively decreases the inertia of momentum of the torsional oscillator, thus increasing the optomechanical coupling strength further.

With feasible experimental parameters, the optomechanical coupling strength can reach the order of 20 kHz, which can be further amplified into the strong coupling regime

*shaoliang@hust.edu.cn
†jianmingcai@hust.edu.cn

[35] (i.e., optomechanical coupling coefficient $\chi \geq 1$) by using a coherent laser to pump one of the orthogonal polarization mode. This enables us to control the torsional quantum state of the torsional oscillator using only a few photons of the other optical mode, even though the original optomechanical coupling strength does not satisfy the usual single-photon strong-coupling condition [36]. Based on this system, it is feasible to prepare the torsional oscillator into a coherent superposition state of two macroscopically distinct torsional quantum states, thus providing a platform to explore the fundamental problems related with quantum torsional motion, such as the macroscopic decoherence, rotational friction, and diffusion of a long quantum torsional oscillator [37,38]. Therefore, our system greatly enriches the toolbox of quantum optomechanics.

This paper is organized as follows. In Sec. II, we derive the general Hamiltonian describing the spin angular-momentum optomechanical system. In Sec. III, we derive the optomechanical input-output relation. In Sec. IV, we prepare our torsional oscillator in squeezed single-phonon state and Schrödinger catlike state. In Sec. V, we discuss the experimental feasibility of our system. A summary is given in Sec. VI.

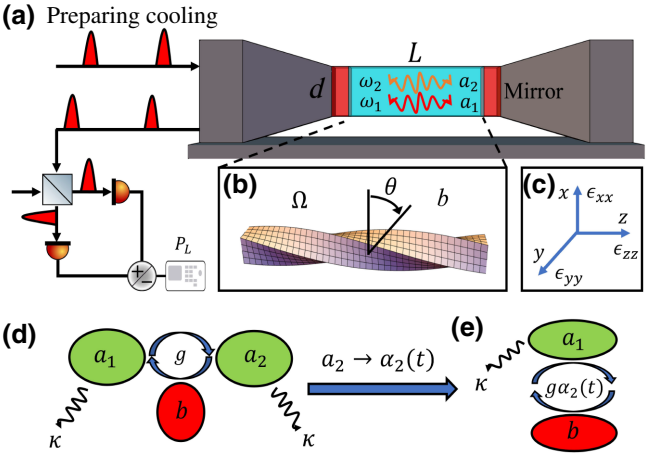

FIG. 1. (a) Sketch showing the experimental embodiment of this optomechanical resonator. (b) The torsional mode of the optomechanical resonator with the relative permittivity ϵ_{ii} (c) in the i ($i = x, y, z$) direction. (d) The optomechanical resonator couples with the two optical modes, the optomechanical coupling strength of which is denoted as g, see Eq. (26). (e) shows the effective coupling between the torsional mode b and the optical mode a_1 when the optical mode a_2 is classically driven by a coherent laser pulse with the characteristic parameter $\alpha_2(t)$.

II. HAMILTONIAN OF SPIN ANGULAR-MOMENTUM OPTOMECHANICAL SYSTEM

A. The general model

The optomechanical resonator that we consider is a suspended square beam [39–41] with length L and width d ($L \gg d$), the basic structure of which is presented in Fig. 1. The optical anisotropy of this optomechanical resonator results in the following relative permittivity tensor ϵ_1:

$$\epsilon_1 = \begin{pmatrix} \epsilon_{xx} & 0 & 0 \\ 0 & \epsilon_{yy} & 0 \\ 0 & 0 & \epsilon_{zz} \end{pmatrix}, \tag{1}$$

where ϵ_{ii} is the relative permittivity in the i ($i = x, y, z$) direction in laboratory frame. This optomechanical resonator supports two fundamental orthogonal quasilinear polarization optical modes with the corresponding electric field profiles $\mathbf{E}_1(\mathbf{x}) = \mathbf{E}_1(x, y)\cos(\beta_1 z)\exp(i\omega_1 t)$ with resonance frequency ω_1 and $\mathbf{E}_2(\mathbf{x}) = \mathbf{E}_2(x, y)\cos(\beta_2 z)\exp(i\omega_2 t)$ with resonance frequency ω_2 [42,43]. The total electric field operator can be written as $\mathbf{E}(\mathbf{x}) = \mathbf{E}_1(\mathbf{x})a_1 + \mathbf{E}_2(\mathbf{x})a_2 + \text{h.c.}$, where a_1 and a_2 are the annihilation operators of two optical modes, which satisfy bosonic commutation relation $[a_i, a_j^\dagger] = \delta_{ij}$ $(i, j = 1, 2)$. The optomechanical resonator can be implemented by α quartz [44] and when $\lambda = 1.55\ \mu$m [45], ϵ_1 is

$$\epsilon(0) = \begin{pmatrix} 1.5326^2 & 0 & 0 \\ 0 & 1.5277^2 & 0 \\ 0 & 0 & 1.5277^2 \end{pmatrix}. \tag{2}$$

In our numerical analysis, we set the cross-section width $d = 1\ \mu$m and the length $L = 100\ \mu$m. The electric field profiles of our system are demonstrated in Fig. 2. We also utilize photonic crystal [40,46,47] to serve as the mirror of our optomechanical resonator and the corresponding optical quality factor $Q_o = 8.4 \times 10^5$.

From a mechanical point of view, the torsional wave in a mechanical oscillator with $L \gg d$ can be described by one-dimensional Webster-type wave equation [48,49]

$$c_t^{-2}\partial_t^2\phi(z,t) - \partial_z^2\phi(z,t) - \left(\frac{\partial_z I_p(z)}{I_p(z)}\right)\partial_z\phi(z,t) = 0, \tag{3}$$

where $I_p(z) = \int_A r^2 dA$ is the polar moment of inertia at the cross section $A(z)$, c_t is the phase velocity of torsional wave, $\phi(z,t) = \theta(z)\cos(\Omega t)$ is the amplitude of angular displacement with Ω the torsional resonance frequency and $\theta(z)$ the spatial mode function of torsional motion, which satisfies the condition $\max|\theta(z)| = 1$. In order to decrease mechanical dissipation [48,50], we focus on the fundamental mode of torsional motion, which can be supposed as $\theta(z) \propto \cos(k_t z)$ [50], where $k_t = \Omega/c_t$ and the exact acoustic velocity c_t depends on the cutting direction

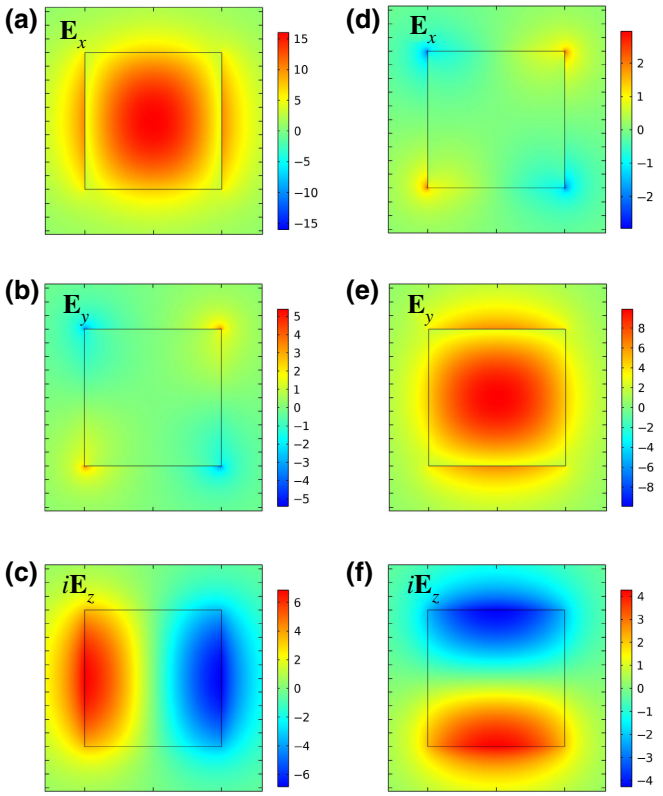

FIG. 2. (a)–(c) are the electric field profiles of the TE-like mode with arbitrary units. (d)–(f) are the electric field profiles of the TM-like mode with arbitrary units. It is obvious that $|\mathbf{E}_i|^2$ $(i = x, y, z)$ is symmetric about the x axis and the y axis.

of this suspended beam [51,52]. By introducing phonon annihilation operator b, we can express the Hamiltonian of the torsional motion as $H_m = \hbar\Omega(b^\dagger b + 1/2)$ [50]. Besides, we assume the displacement vector $\mathbf{u}(\mathbf{x})$ of the torsional motion [50] is given by $\mathbf{u}(\mathbf{x}) = \theta(z)(r/R)\hat{\boldsymbol{\theta}} = \theta(z)(-y\hat{\mathbf{x}} + x\hat{\mathbf{y}})/R$ in cylindrical and Cartesian coordinates, respectively. Here the constant R enables $\mathbf{u}(\mathbf{x})$ to satisfy the condition $\max|\mathbf{u}(\mathbf{x})| = 1$.

For a suspended square beam with uniform mass density $\rho = 2650$ kg/m^3, the effective moment of inertia is estimated to be $I_{\text{eff}} \sim 10 I_{\text{beam}} = (5/3)\rho d^4 \int_{-L/2}^{L/2} \theta(z)^2 dz = (5/6)\rho L d^4 \approx 4.4 \times 10^{-25}$ kg m^2. Besides, we choose the fundamental mode torsional resonance frequency $\Omega = 2\pi \times 500$ kHz, the mechanical quality factor $Q_m = 10^6$ [27,44,48,53–56] and $c_t = 5.0$ km s^{-1}. The parameters used in the calculation are listed in Table I.

B. Coupling among electromagnetic field and mechanical motion

The Hamiltonian of electromagnetic field can be written as $H_{\text{em}} = 1/2 \int_V dV[\epsilon_0 \mathbf{E}(\mathbf{x}) \cdot \epsilon_1(\mathbf{x})\mathbf{E}(\mathbf{x}) + \mu_0 \mathbf{H}(\mathbf{x}) \cdot \mu(\mathbf{x})\mathbf{H}(\mathbf{x})]$ [57]. The torsional motion of the optomechanical resonator will influence the relative permittivity ϵ, and thus affect the Hamiltonian H_{em}. If we neglect optoelastic effect [58,59] and moving boundary effect [59,60], the relative permittivity $\epsilon(\theta)$ of the torsional motion can be estimated as

$$\epsilon_1(\theta) = R(\theta)\epsilon_1(0)R(-\theta), \tag{4}$$

where $\epsilon_1(0) = \epsilon_1$ and

$$R(\theta) = \begin{pmatrix} \cos(\theta) & -\sin(\theta) & 0 \\ \sin(\theta) & \cos(\theta) & 0 \\ 0 & 0 & 1 \end{pmatrix}$$

is a rotation matrix along the z axis. Expanding $R(\theta)$ to the first order of θ, we can derive the approximated expression of $\epsilon(\theta)$ as

$$\epsilon_1(\theta) = \epsilon_1(0) + \delta\epsilon\theta(z)A, \tag{5}$$

where $\delta\epsilon = \epsilon_{xx} - \epsilon_{yy}$ and

$$A = \begin{pmatrix} 0 & 1 & 0 \\ 1 & 0 & 0 \\ 0 & 0 & 0 \end{pmatrix}.$$

The matrix A mixes two optical modes a_1 and a_2 in Hamiltonian H_{em} and induces exchange interaction between the optical modes a_1 and a_2. Therefore, the optomechanical interaction Hamiltonian

$$\begin{aligned} H_{\text{int}} &\propto \epsilon_0 \delta\epsilon \int_V dV\theta(z)\mathbf{E}(\mathbf{x}) \cdot A\mathbf{E}(\mathbf{x}) \\ &\propto \hbar g(b + b^\dagger)a_1^\dagger a_2 + \hbar g^*(b + b^\dagger)a_2^\dagger a_1, \end{aligned} \tag{6}$$

where g is the optomechanical coupling strength.

For realistic optomechanical systems, the influences of optoelastic effect and moving boundary coupling effect must also be taken into account. We consider a dielectric material with permittivity $\epsilon(\mathbf{x}) = \epsilon_1$ in a volume V_1, which is localized in a surrounding medium with permittivity $\epsilon(\mathbf{x}) = \epsilon_2$ occupying the complementary volume V_2,

TABLE I. Parameters used in the calculation.

$d/\ \mu$m	$L/\ \mu$m	ρ/kg m^{-3}	Ω/kHz	c_t/km s^{-1}	β_1/k	β_2/k	Q_m	Q_o
1	100	2650	$2\pi \times 500$	5.0	1.2859	1.2926	10^6	8.4×10^6

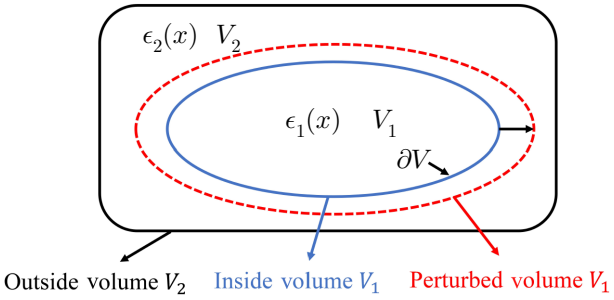

FIG. 3. A dielectric material with permittivity ϵ_1 in a volume V_1 (blue circle) is surrounded by a medium with permittivity ϵ_2 occupying the complementary volume V_2 (black circle). The perturbed volume is represented by the dashed red circle and ∂V is the boundary between V_1 and V_2.

see Fig. 3. Noting that the unperturbed permittivity can be written as

$$\epsilon(\mathbf{x}) = \epsilon_2 + (\epsilon_1 - \epsilon_2)\,\Theta(\mathbf{x}), \tag{7}$$

where $\Theta(\mathbf{x})$ is a step function defined by

$$\Theta(\mathbf{x}) = \begin{cases} 1 & \text{for} \quad \mathbf{x} \in V_1 \\ 0 & \text{for} \quad \mathbf{x} \in V_2. \end{cases} \tag{8}$$

The mechanical motion of the dielectric material will influence the total permittivity $\epsilon(\mathbf{x})$. We assume that $\epsilon_1 = \epsilon_1[\mathbf{x}, \alpha\mathbf{u}(\mathbf{x})] = \epsilon_1(\mathbf{x}, \alpha)$, where α is the amplitude of the mechanical motion and α is much smaller than the scale of the optomechanical resonator. When $\alpha = 0$, $\epsilon_1(\mathbf{x}, \alpha)|_{\alpha=0} = \epsilon_1(\mathbf{x})$, which is the unperturbed value of ϵ_1. Then the perturbed permittivity can be further written as

$$\epsilon(\mathbf{x}, \alpha) = \epsilon_2 + [\epsilon_1(\mathbf{x}, \alpha) - \epsilon_2]\,\Theta(\mathbf{x} + \alpha\mathbf{u}). \tag{9}$$

Expanding $\epsilon(\mathbf{x}, \alpha)$ to the first order of α, we have

$$\begin{aligned} \epsilon(\mathbf{x}, \alpha) &\approx \epsilon_2 + \left[\epsilon_1(\mathbf{x}, 0) - \epsilon_2 + \alpha \frac{\partial \epsilon_1(\mathbf{x}, \alpha)}{\partial \alpha}\bigg|_{\alpha=0}\right] \\ &\quad \times [\Theta(\mathbf{x}) + \alpha\mathbf{u}(\mathbf{x}) \cdot \nabla\Theta(\mathbf{x})] \\ &\approx \epsilon(\mathbf{x}) + \alpha\,(\epsilon_{\mathrm{MB}} + \epsilon_{\mathrm{other}}), \end{aligned} \tag{10}$$

where

$$\epsilon_{\mathrm{MB}} = (\epsilon_1(\mathbf{x}, 0) - \epsilon_2)\,\mathbf{u}(\mathbf{x}) \cdot \nabla\Theta(\mathbf{x}), \tag{11}$$

and

$$\epsilon_{\mathrm{other}} = \frac{\partial \epsilon_1(\mathbf{x}, \alpha)}{\partial \alpha}\bigg|_{\alpha=0} \Theta(\mathbf{x}). \tag{12}$$

According to Refs. [59,60], the optomechanical interaction Hamiltonian induced by ϵ_{MB} is

$$\begin{aligned} H_{\mathrm{MB}} &= \frac{1}{2}\alpha \int dV \mathbf{E}(\mathbf{x})^\dagger \epsilon_{\mathrm{MB}} \mathbf{E}(\mathbf{x}) \\ &= \frac{1}{2}\alpha \int_{\partial V} d\mathbf{A} \cdot \mathbf{u}(\mathbf{x})[-\mathbf{E}_\parallel(\mathbf{x})^\dagger \Delta\epsilon \mathbf{E}_\parallel(\mathbf{x}) \\ &\quad + \mathbf{D}_\perp(\mathbf{x})^\dagger \Delta(\epsilon^{-1}) \mathbf{D}_\perp(\mathbf{x})], \end{aligned} \tag{13}$$

where $\Delta\epsilon = \epsilon_1 - \epsilon_2$, $\Delta\left(\epsilon^{-1}\right) = \epsilon_1^{-1} - \epsilon_2^{-1}$, $\mathbf{E}_\parallel$ is the electric field, which is parallel with the surface of V_1 and $\mathbf{D}_\perp$ is the electric displacement field, which is perpendicular with the surface of V_1. It is obvious that Hamiltonian H_{MB} is just the moving boundary coupling optomechanical Hamiltonian [59,60].

Dielectric permittivity $\epsilon_1(\mathbf{x}, \alpha)$ will also be modified by optoelastic effect when material is subject to strain. Mathematically, optoelastic effect is described by relating the change of the permittivity tensor $\delta\eta$ to the material strain by Pockel's tensor p [61], $(\boldsymbol{\delta}\eta)_{ij} = p_{ijkl} s_{kl}$, where s_{mn} is the strain tensor of the material with $s_{mn} = \frac{1}{2}\left(\partial \mathbf{u}_m/\partial \mathbf{x}_n + \partial \mathbf{u}_n/\partial \mathbf{x}_m\right)$. The modified permittivity tensor follows the equation $\epsilon^{\mathrm{OE}} = \left(\epsilon^{-1} + \alpha\delta\eta\right)^{-1}$, where ϵ is the unmodified permittivity tensor. Considering Eq. (4), the finally expression of $\epsilon_1^{\mathrm{OE}}(\mathbf{x}, \alpha)$ is

$$\begin{aligned} \epsilon_1^{\mathrm{OE}}(\mathbf{x}, \alpha) &= (\epsilon_1(\mathbf{x}, \alpha)^{-1} + \alpha\delta\eta)^{-1} \\ &= \left(R(\alpha\theta)\epsilon_1^{-1}(\mathbf{x}, 0)R(-\alpha\theta) + \alpha\delta\eta\right)^{-1} \\ &\approx \epsilon_1(\mathbf{x}, 0) + \alpha\theta\delta\epsilon A - \alpha\epsilon_1(\mathbf{x}, 0)\delta\eta\epsilon_1(\mathbf{x}, 0). \end{aligned} \tag{14}$$

As a consequence, we have

$$\begin{aligned} \epsilon_{\mathrm{other}} &= \frac{\partial \epsilon_1^{\mathrm{OE}}(\mathbf{x}, \alpha)}{\partial \alpha}\Theta(\mathbf{x}) \\ &= \theta[T, \epsilon_1(\mathbf{x}, 0)]\Theta(\mathbf{x}) - \epsilon_1(\mathbf{x}, 0)\delta\eta\epsilon_1(\mathbf{x}, 0)\Theta(\mathbf{x}) \\ &= \epsilon_{\mathrm{MA}} + \epsilon_{\mathrm{OE}}, \end{aligned} \tag{15}$$

where the first term $\epsilon_{\mathrm{MA}} = \theta\delta\epsilon A\Theta(\mathbf{x})$ (MA stands for material anisotropy) is related with the optical anisotropy $\delta\epsilon$ and the second term $\epsilon_{\mathrm{OE}} = -\epsilon_1(\mathbf{x}, 0)\delta\eta\epsilon_1(\mathbf{x}, 0)\Theta(\mathbf{x})$ is related with the optoelastic effect. Therefore, the optomechanical interaction Hamiltonian H_{other} can be divided into two terms

$$H_{\mathrm{MA}} = \frac{1}{2}\alpha\delta\epsilon \int_{V_1} dV\theta(z)\mathbf{E}(\mathbf{x})^\dagger A \mathbf{E}(\mathbf{x}), \tag{16}$$

and

$$H_{\mathrm{OE}} = -\frac{1}{2}\alpha \int_{V_1} dV \mathbf{E}(\mathbf{x})^\dagger \epsilon_1(\mathbf{x}, 0)\delta\eta\epsilon_1(\mathbf{x}, 0)\mathbf{E}(\mathbf{x}). \tag{17}$$

TABLE II. Optomechanical coupling strength.

$g_{12\mathrm{MA}}$/kHz	$g_{11\mathrm{MA}}$/kHz	$g_{22\mathrm{MA}}$/kHz	$g_{12\mathrm{MB}}$/kHz	$g_{11\mathrm{MB}}$/kHz	$g_{22\mathrm{MB}}$/kHz	$g_{ij\,\mathrm{OE}}$/kHz
22	0	0	0.081	−0.01	−0.01	0

C. Quantization

To date, we derive the classical expressions of optomechanical Hamiltonians H_{MB}, H_{OE}, and H_{MA}. We define $x_{\mathrm{ZP}} = \sqrt{\hbar/(2m_{\mathrm{eff}}\Omega)}$, which is the zero-point linear displacement of the optomechanical resonator and $\theta_{\mathrm{ZP}} = \sqrt{\hbar/(2I_{\mathrm{eff}}\Omega)}$, which is the zero-point angular displacement of the optomechanical resonator. Then the quantized Hamiltonians can be obtained by replacing $\alpha\mathbf{u}(\mathbf{x})$ with operator $x_{\mathrm{ZP}}(b+b^\dagger)\mathbf{u}(\mathbf{x})$, $\alpha\theta(z)$ with operator $\theta_{\mathrm{ZP}}(b+b^\dagger)\theta(z)$ and the classical electromagnetic fields with electromagnetic fields operators. Therefore, the original optomechanical Hamiltonian H_{int} is

$$H_{\mathrm{int}} = H_{\mathrm{MB}} + H_{\mathrm{OE}} + H_{\mathrm{MA}} = \hbar(b+b^\dagger)\sum_{i,j=1,2} a_i^\dagger a_j g_{ij}, \tag{18}$$

where $g_{ij} = g_{ij\,\mathrm{MB}} + g_{ij\,\mathrm{OE}} + g_{ij\,\mathrm{MA}}$,

$$g_{ij\,\mathrm{MB}} = \frac{x_{\mathrm{ZP}}}{2}\int_{\partial V} d\mathbf{A}\cdot\mathbf{u}(\mathbf{x})[-\mathbf{E}_{i\parallel}(\mathbf{x})^\dagger\Delta\epsilon\mathbf{E}_{j\parallel}(\mathbf{x}) + \mathbf{D}_{i\perp}(\mathbf{x})^\dagger\Delta(\epsilon^{-1})\mathbf{D}_{j\perp}(\mathbf{x})], \tag{19}$$

$$g_{ij\,\mathrm{OE}} = -\frac{x_{\mathrm{ZP}}}{2}\int_{V_1} dV\mathbf{E}_i(\mathbf{x})^\dagger\epsilon_1(\mathbf{x},0)\delta\eta\epsilon_1(\mathbf{x},0)\mathbf{E}_j(\mathbf{x}), \tag{20}$$

and

$$g_{ij\,\mathrm{MA}} = \frac{1}{2}\theta_{\mathrm{ZP}}\delta\epsilon\int_{V_1} dV\theta(z)[E_{iy}(\mathbf{x})E_{jx}^*(\mathbf{x}) + E_{jy}^*(\mathbf{x})E_{ix}(\mathbf{x})]. \tag{21}$$

Although H_{int} involves several optomechanical coupling strengths $g_{ij}\,(i,j=1,2)$, for our optomechanical system, only $g_{12\mathrm{MA}}(g_{21\mathrm{MA}}^*)$ will contribute to H_{int}.

Firstly, we prove that $g_{11\mathrm{MB}} \approx 0$ and $g_{22\mathrm{MB}} \approx 0$. Because of the symmetry of our optomechanical resonator, $|\mathbf{E}_{i\parallel}(\mathbf{x})|^2$ and $|\mathbf{D}_{i\perp}(\mathbf{x})|^2$ $(i=1,2)$ will be even functions about x axis and y axis. However, torsional mode function $\mathbf{u}(\mathbf{x})$ is an odd function about the x axis and the y axis. Therefore, the integration about $g_{ij\,\mathrm{MB}}$ will approach 0.

Secondly, we prove that $g_{12\mathrm{MB}} \approx 0$. From Fig. 2 we know that $\mathbf{E}_1(\mathbf{x})$ is a quasi-x-polarized electric field with $|E_{1y}| \ll |E_{1x}|$ and $\mathbf{E}_2(\mathbf{x})$ is a quasi-y-polarized electric field with $|E_{2x}| \ll |E_{2y}|$. Besides, $\mathbf{E}_{1\parallel}(\mathbf{x})^\dagger\Delta\epsilon\mathbf{E}_{2\parallel}(\mathbf{x})$ can be expanded into the summation of $E_{1m}(\mathbf{x})^\dagger\Delta\epsilon E_{2m}(\mathbf{x})$ $(m = x,y,z)$. Then we have

$$g_{12\mathrm{MB}} \propto \sum_{m=x,y,z}\frac{\int\left(-E_{1m}^*\Delta\epsilon E_{2m} + D_{1m}^*\Delta(\epsilon^{-1})D_{2m}\right)dA}{\sqrt{\int\mathbf{E}_1\cdot\epsilon\mathbf{E}_1 dA}\cdot\sqrt{\int\mathbf{E}_2\cdot\epsilon_2\mathbf{E}_2 dA}} \approx 0. \tag{22}$$

Besides, the reason that $g_{ii\mathrm{MA}} \approx 0 (i=1,2)$ is similar with the reason that $g_{12\mathrm{MB}} \approx 0$ and we will not repeat this process.

Thirdly, we prove $g_{ij\,\mathrm{OE}} \approx 0 (i,j=1,2)$. The exact values of $g_{ij\,\mathrm{OE}}$ depends on the strain tensor s_{mn}, electric field $\mathbf{E}_1(\mathbf{x})$, and electric field $\mathbf{E}_2(\mathbf{x})$. When the mode function $\theta(z) = \cos(k_t z)$, the strain tensor s_{mn} is

$$\mathbf{s} = \frac{1}{2}\sin(k_t z)\frac{k_t}{R}\begin{pmatrix}0 & 0 & y\\ 0 & 0 & -x\\ y & -x & 0\end{pmatrix}. \tag{23}$$

Considering $\mathbf{E}_i(\mathbf{x}) = \mathbf{E}_i(x,y)\cos(\beta_i z)$, we have

$$g_{ij\,\mathrm{OE}} \propto \int_{-L/2}^{L/2}\sin(k_t z)\cos(\beta_i z)\cos(\beta_j z)dz = 0. \tag{24}$$

Noting that here we do not need the exact value of Pockel's tensor p.

Fourthly, taking into the normalization condition of the electric fields, we can express $g_{12\mathrm{MA}}$ as

$$g_{12\mathrm{MA}} \propto \theta_{\mathrm{ZP}}\sqrt{\omega_1\omega_2}\left(\frac{\delta\epsilon}{L}\right)\int_{-L/2}^{L/2}\theta(z)\cos(\beta_1 z)\cos(\beta_2 z)dz. \tag{25}$$

The exact expression of $g_{12\mathrm{MA}}$ is listed in Appendix C. Obviously, $g_{12\mathrm{MA}}$ is proportional to the optical anisotropy $\delta\epsilon$ of the torsional oscillator, see Eq. (25). Besides, the integral factor in Eq. (25) is determined by the wave vectors β_1 and β_2 of the two optical modes and the wave vector k_t of the torsional mode. The exact values of these optomechanical coupling strength are listed in Table II.

Finally, we can obtain the total optomechanical Hamiltonian as

$$H_{\mathrm{OM}} = \hbar\Omega b^\dagger b + \hbar\omega_1 a_1^\dagger a_1 + \hbar\omega_2 a_2^\dagger a_2 + \hbar g(b+b^\dagger)a_1^\dagger a_2 + \hbar g^*(b+b^\dagger)a_2^\dagger a_1, \tag{26}$$

where $g = g_{12\mathrm{MA}} + g_{12\mathrm{MB}} + g_{12\mathrm{OE}}$ is the optomechanical coupling strength. Even if moving boundary coupling

effect [59,60] and optoelastic coupling effect [58,59] will also contribute to g, our analysis has shown that the contributions of these effects are much less significant than the contribution of the optical anisotropy and can be neglected in the present system.

III. OPTOMECHANICAL INPUT-OUTPUT RELATION

A. Effective optomechanical Hamiltonian

To achieve strong optomechanical coupling at the single-photon level, we set two optical modes a_1 and a_2 as degenerate with $\omega_1 = \omega_2$ [62]. Then the Hamiltonian $H_{\rm OM}$ in Eq. (26) can be expressed in interaction picture as $H_{\rm OM} = \hbar g(be^{-i\Omega t} + b^\dagger e^{i\Omega t})(a_1^\dagger a_2 + a_2^\dagger a_1)$. If we utilize a strong coherent laser with duration τ to pump the optical mode a_2, the corresponding the Langevin equation is

$$\dot{a}_2 = -\frac{\kappa}{2}a_2 - \sqrt{2}g\theta_M a_1 + \sqrt{\kappa}a_{2\rm in}(t), \tag{27}$$

where κ is the decaying rate of the cavity. Considering the fact that the intensity of $a_2(t)$ is extremely large, we can reasonably neglect weak coupling term $\sqrt{2}g\theta_M a_1$. In our following discussion, we consider only the classical amplitude α_2 of mode a_2. When $\kappa \gg \tau^{-1}$, the dynamics of the intracavity field a_2 can be eliminated adiabatically, which means that

$$\frac{d\alpha_2(t)}{dt} \approx -\frac{\kappa}{2}a_2 + \sqrt{\kappa}a_{2\rm in}(t) \approx 0, \tag{28}$$

Then a simple relation between the external and internal field amplitudes can be yielded

$$\alpha_2(t) = \frac{2}{\sqrt{\kappa}}\alpha_{2\rm in}(t). \tag{29}$$

where $\alpha_{2\rm in}(t)$ is the average value of $a_{2\rm in}$. We assume the temporal function of $a_{2\rm in}(t)$ is $f(t)$, which has an envelop with duration τ and satisfies the normalized condition $\int_{-\infty}^{\infty} f(t)^2 dt = 1$. If the photon number of a single pulse is $N_{\rm in}$, then $\alpha_{2\rm in}$ will become $\alpha_{2\rm in}(t) = \sqrt{N_{\rm in}}f(t)$. At this case, $\alpha_2(t)$ can be expressed as

$$\alpha_2(t) = \frac{2}{\sqrt{\kappa}}\alpha_{2\rm in}(t) = 2\sqrt{\frac{N_{\rm in}}{\kappa}}f(t) = \alpha f(t), \tag{30}$$

where $\alpha = 2\sqrt{N_{\rm in}/\kappa}$. Then the Hamiltonian $H_{\rm OM}$ becomes

$$H_{\rm OM}^{\rm new} = \hbar g\alpha_2(t)(be^{-i\Omega t} + b^\dagger e^{i\Omega t})(a_1^\dagger + a_1). \tag{31}$$

By defining $x_L = (a_1^\dagger + a_1)/\sqrt{2}$, $p_L = i(a_1^\dagger - a_1)/\sqrt{2}$, $\theta_M = (b^\dagger + b)/\sqrt{2}$, $L_M = i(b^\dagger - b)/\sqrt{2}$, the Hamiltonian $H_{\rm OM}^{\rm new}$ becomes $H_{\rm OM}^{\rm new} = 2\hbar g\alpha_2(t)x_L[\theta_M\cos(\Omega t) + L_M\sin(\Omega t)]$. When the condition $\Omega \ll \tau^{-1} \ll \kappa$ is satisfied, we can neglect the second term of the Hamiltonian $H_{\rm OM}^{\rm new}$ and obtain the following effective Hamiltonian as

$$H_{\rm eff} = 2\hbar g\alpha_2(t)x_L\theta_M. \tag{32}$$

This above Hamiltonian $H_{\rm eff}$ describes the effective interaction between the optical mode a_1 and the torsional mode b.

B. Input-output relation

Based on Eq. (32), we can describe the dynamics of the optical and mechanical quadrature operators by the set of the following Langevin equations:

$$\begin{aligned}
\frac{dx_L(t)}{dt} &= -\frac{\kappa}{2}x_L(t) + \sqrt{\kappa}x_L^{\rm in}(t),\\
\frac{dp_L(t)}{dt} &= -2g\alpha_2(t)\theta_M - \frac{\kappa}{2}p_L(t) + \sqrt{\kappa}p_L^{\rm in}(t),\\
\frac{d\theta_M}{dt} &= 0,\\
\frac{dL_M}{dt} &= -2g\alpha_2(t)x_L(t),
\end{aligned} \tag{33}$$

where $x_L^{\rm in}(t)$ and $p_L^{\rm in}(t)$ are the quadratures of input noise, which satisfy the commutation relation $\left[x_L^{\rm in}(t), p_L^{\rm in}\left(t'\right)\right] = i\delta\left(t - t'\right)$. Invoking adiabatic elimination of the optical intracavity field $dx_L(t)/dt \approx 0$ and $dp_L(t)/dt \approx 0$, we have the following equations:

$$\begin{aligned}
x_L(t) &= \frac{2}{\sqrt{\kappa}}x_L^{\rm in}(t),\\
p_L(t) &= \frac{2}{\sqrt{\kappa}}p_L^{\rm in}(t) - \frac{4g\alpha_2(t)}{\kappa}\theta_M.
\end{aligned} \tag{34}$$

By means of the usually optical input-output relation $a_1^{\rm out}(t) + a_1^{\rm in}(t) = \sqrt{\kappa}a_1(t)$ we find

$$\begin{aligned}
x_L^{\rm out}(t) &= x_L^{\rm in}(t),\\
p_L^{\rm out}(t) &= p_L^{\rm in}(t) - \frac{4g\alpha_2(t)}{\sqrt{\kappa}}\theta_M(t),\\
\frac{d\theta_M}{dt} &= 0,\\
\frac{dL_M}{dt} &= -2g\alpha_2(t)x_L(t).
\end{aligned} \tag{35}$$

In order to derive optomechanical input-output relation, we define time collective optical quadratures $x_L^{\rm in/out} = \int_{-\infty}^{\infty} f(t)x_L^{\rm in/out}(t)dt$, $p_L^{\rm in/out} = \int_{-\infty}^{\infty} f(t)p_L^{\rm in/out}(t)dt$. It is easy to verify that $x_L^{\rm in/out}$ and $p_L^{\rm in/out}$ also satisfy the standard commutation $\left[x_L^{\rm in/out}, p_L^{\rm in/out}\right] = i$. Besides, we define $\theta_M^{\rm in} = \theta_M(t = -\infty)$ and $\theta_M^{\rm out} = \theta_M(t = +\infty)$. As $\alpha_2(t)$ is a short

pulse, $\theta_M^{\rm in}$ and $\theta_M^{\rm out}$ represent the θ_M quadrature before and after the optomechanical interaction, respectively.

Firstly, from equation $d\theta_M/dt = 0$, we can get the conclusion that $\theta_M(t) = \theta_M^{\rm in} = \theta_M^{\rm out}$, which means $\theta_M(t)$ is a constant operator during the optomechanical interaction. Secondly, multiplying the equation $x_L^{\rm out}(t) = x_L^{\rm in}(t)$ by $f(t)$ and integrating it over the whole time interval, we obtain the equation $x_L^{\rm out} = x_L^{\rm in}$. Similarly, also multiplying the equation $p_L^{\rm out}(t) = p_L^{\rm in}(t) - 4g\theta_M\alpha_2(t)/\sqrt{\kappa}$ by $f(t)$ and integrating it over the whole time interval, we have $p_L^{\rm out} = p_L^{\rm in} - (4g/\sqrt{\kappa})\int_{-\infty}^{\infty} f(t)\alpha_2(t)\theta_M(t)dt = p_L^{\rm in} - (4g\theta_M^{\rm in}/\sqrt{\kappa})\int_{-\infty}^{\infty} f(t)\alpha_2(t)dt$.

Defining $\chi = (4g/\sqrt{\kappa})\int_{-\infty}^{\infty} f(t)\alpha_2(t)dt$, and considering $\alpha_2(t) = \alpha f(t)$, we have

$$\chi = \frac{4g}{\sqrt{\kappa}}\int_{-\infty}^{\infty} f(t)\alpha_2(t)dt = \frac{8g\sqrt{N_{\rm in}}}{\kappa}. \tag{36}$$

As a consequence, we have $p_L^{\rm out} = p_L^{\rm in} - \chi\theta_M^{\rm in}$. Thirdly, from equation $dL_M/dt = -2g\alpha_2(t)x_L(t)$, we know that $L_M^{\rm out} - L_M^{\rm in} = -2g\int_{-\infty}^{\infty}\alpha_2(t)x_L(t)$. Using Eq. (34), we have $L_M^{\rm out} - L_M^{\rm in} = -(4g/\sqrt{\kappa})\int_{-\infty}^{\infty}\alpha_2(t)x_L^{\rm in}(t)dt = -(4g\alpha/\sqrt{\kappa})x_L^{\rm in} = -\chi x_L^{\rm in}$.

Finally, we have the following input-output relation [63–67]:

$$\begin{aligned} x_L^{\rm out} &= x_L^{\rm in}, \\ p_L^{\rm out} &= p_L^{\rm in} - \chi\theta_M^{\rm in}, \\ \theta_M^{\rm out} &= \theta_M^{\rm in}, \\ L_M^{\rm out} &= L_M^{\rm in} - \chi x_L^{\rm in}. \end{aligned} \tag{37}$$

Through this optomechanical interaction, the optical quadratures x_L and p_L partially exchanges information with the torsional quadratures θ_M and L_M. Therefore, the torsional oscillator becomes correlated with the optical mode a_1. It is worthwhile to note that our spin angular-momentum optomechanical interaction (26) makes the input-output relation (37) without a classical momentum term, which usually occurs in linear momentum optomechanical systems [63,64,66], therefore, we do not need to compensate for the influence induced by the classical momentum term.

Noting that when $\chi \geq 1$, Eq. (37) allows an effective coherent control of the torsional oscillator by very few photons of the optical mode a_1, and thus provides a platform to realize single-photon optomechanics [36], even though this system does not satisfy the usually single-photon strong-coupling condition $g \geq \Omega$ [36]. The requirement for the realization of single-photon optomechanics, namely to achieve $\chi \geq 1$ is $N_{\rm in} \geq 6.45 \times 10^7$, which is feasible in the state-of-the art experiment [35,64].

As powered by the strong single-photon optomechanical coupling with $\chi \geq 1$, the torsional oscillator can be squeezed and cooled efficiently in this system using a single-pulse-measurement protocol [64]. By pumping mode a_2 with a single coherent pulse and then performing a homodyne detection on quadrature $p_L^{\rm out}$, the torsional oscillator will be projected into a state that inherits the features of the input state of the optical mode a_1. As an example, we assume that the input state of the optical mode a_1 is a vacuum state, and the input state of the torsional oscillator is a thermal state with the mean phonon number $\bar{n}$. According to the input-output relation Eq. (37) and noticing that $\Delta\left(p_L^{\rm out}\right)$, the variance of $p_L^{\rm out}$ becomes 0 by the homodyne detection, we obtain

$$\begin{aligned} \Delta(\theta_M^{\rm out})^2 &= \chi^{-2}\Delta\left(p_L^{\rm in}\right)^2 + \chi^{-2}\Delta\left(p_L^{\rm out}\right)^2 = 1/(2\chi^2), \\ \Delta(L_M^{\rm out})^2 &= \Delta\left(L_M^{\rm in}\right)^2 + \chi^2\Delta\left(x_L^{\rm in}\right)^2 = (\bar{n} + 1/2) + \chi^2/2. \end{aligned} \tag{38}$$

Therefore, when $\chi \geq 1$, $\Delta(\theta_M^{\rm out})^2 = 1/(2\chi^2) \leq 1/2$, the θ_M quadrature is thus squeezed to the level of the vacuum fluctuation and L_M quadrature is almost unaffected. As a consequence, this torsional oscillator is squeezed into an asymmetrically cooled state (namely squeezed thermal state) [64,65].

IV. PREPARATION OF NON-GAUSSIAN AND NONCLASSICAL QUANTUM STATES

A. General preparation process

In this section, we discuss the preparation process of the non-Gaussian and nonclassical quantum states of our torsional oscillator. Due to the quintessential embodiment of the manifestly nonclassical properties of quantum mechanics, Schrödinger cat state and single-phonon state have been widely researched [68–70]. However, it is still very difficult to prepare the motion degree of macroscopic objects in cat state or single-phonon state. Here we demonstrate that the torsional oscillator can be prepared in a Schrödinger catlike state and squeezed single-phonon state using a two-pulse-measurement protocol, see Fig. 4. The first pulse is used to cool the torsional oscillator, as we have explained before. The second set of pulses includes a coherent laser pulse (to pump the mode a_2) and an optical catlike state pulse [71] (to pump the mode a_1) or a single-photon state pulse. The subsequent homodyne measurement on the output field $p_L^{\rm out}$ will partially transfer the quantum state from the optical mode a_1 to the torsional oscillator, thus preparing the torsional oscillator into a Schrödinger catlike state or squeezed single-phonon state.

We use Wigner function to characterize the state of the torsional oscillator. In the Heisenberg picture, if the time evolution of all the quadratures $\mathbf{r}$ of a continuous-variable system can be described by a linear transformation

$$\mathbf{r}(T) = M\mathbf{r}(0), \tag{39}$$

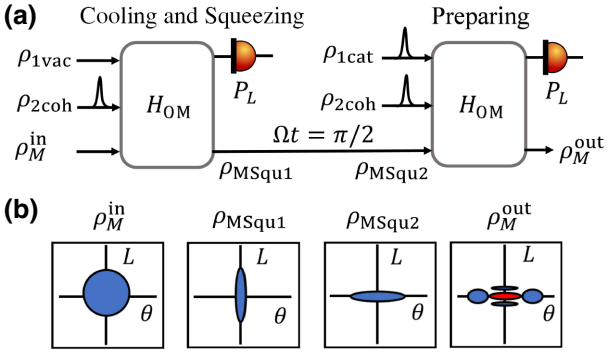

FIG. 4. (a) Protocol for the preparation of macroscopic Schrödinger catlike state of the torsional resonator includes three steps: (1) the torsional resonator is cooled and squeezed ($\rho_M^{\mathrm{in}} \to \rho_{\mathrm{MSqu1}}$) by the first optomechanical interaction H_{OM} and the homodyne detection of the $\hat{p}_L^{\mathrm{out}}$ quadrature of the optical mode a_1 (P_L) with the input optical state $\rho_{1\mathrm{vac}}$ (vacuum state) and $\rho_{2\mathrm{coh}}$ (coherent state pulse); (2) the free evolution of the torsional resonator for time $\Omega t = \pi/2$ ($\rho_{\mathrm{MSqu1}} \to \rho_{\mathrm{MSqu2}}$); (3) the torsional resonator is prepared into a Schrödinger catlike state ($\rho_{\mathrm{MSqu2}} \to \rho_M^{\mathrm{out}}$) by the second optomechanical interaction H_{OM} and the homodyne detection of the optical mode a_1 (P_L) with the input optical cat state $\rho_{1\mathrm{cat}}$ and $\rho_{2\mathrm{coh}}$ (coherent state pulse). (b) illustrates the Wigner functions of the mechanical state of the torsional resonator during the experimental protocol.

then at time $T = t$, the Wigner function of the total system is

$$W(\mathbf{r}, T) \propto W(M^{-1}\mathbf{r}, 0). \tag{40}$$

This equation connects the Wigner function at time $t = T$ and at time $t = 0$ (see Appendix A for more details). For our optomechanical system, the input-out relation (37) provides us with a transformation matrix M

$$M = \begin{pmatrix} 1 & 0 & 0 & 0 \\ 0 & 1 & -\chi & 0 \\ 0 & 0 & 1 & 0 \\ -\chi & 0 & 0 & 1 \end{pmatrix}. \tag{41}$$

We assume the initial quantum state $\rho(0) = \rho_L \otimes \rho_M$, where ρ_L is the density matrix of the input optical mode $a_{1\mathrm{in}}$ and ρ_M is the density matrix of the mechanical mode. The corresponding initial Wigner function is $W(\mathbf{r}, 0) = W_L(x_L, p_L) W_M(x_M, p_M)$. After the optomechanical interaction (37), the Wigner function of this system is

$$\begin{aligned} W(\mathbf{r}, T) &= W(M^{-1}\mathbf{r}, 0) \\ &= W_L(x_L, p_L + \chi x_M) W_M(x_M, p_M + \chi x_L). \end{aligned} \tag{42}$$

Through this process, the torsional oscillator becomes correlated with the output mode of a_1.

Then if we perform quantum measurement on the subsystem ρ_L with a measurement operator Π, the resulting Wigner function will be [72]

$$W_{\mathrm{meas}}(x_M, p_M) \propto \int d^2\mathbf{r}_L W(\mathbf{r}) W_\Pi(x_L, p_L), \tag{43}$$

where $W_\Pi(x_L, p_L)$ is the Wigner function of the measurement operator Π. Furthermore, the corresponding success probability [72] is

$$P_\Pi = \iint dx_M dx_L dp_M dp_L W(\mathbf{r}) W_\Pi(x_L, p_L). \tag{44}$$

For perfect homodyne detection, the corresponding Wigner measurement function [72] is

$$W_{\mathrm{homo}}(x_L, p_L) \propto \delta(p_L - p), \tag{45}$$

where p is the result of measurement.

B. Squeezed single-phonon state

We use the two-pulse-measurement protocol to prepare our torsional oscillator into squeezed single-phonon state. Given the input optical single-photon state of mode a_1 with the Wigner function $W_L(x_L, p_L) \propto \exp(-\frac{1}{2}x_L^2 - \frac{1}{2}p_L^2)(x_L^2 + p_L^2 - 1)$ and a precooled mechanical state with the Wigner function $W_M(\theta_M, L_M) \propto \exp\left[-\theta_M^2/(2V_{\theta\theta}) - L_M^2/(2V_{LL})\right]$, where V_{LL} and $V_{\theta\theta}$ are the variance of L_M and θ_M, respectively, the Wigner function of the resulting mechanical state $W(\theta_M, L_M)$ is

$$\begin{aligned} W(\theta_M, L_M) = \iint & dx_L dp_L W_L(x_L, p_L + \chi\theta_M) \\ & \times W_M(\theta_M, L_M + \chi x_L) W_{\mathrm{homo}}(x_L, p_L). \end{aligned} \tag{46}$$

If we choose $\chi = 1$, the success probability can be calculated by Eq. (44) and the exact expression is

$$P_\Pi(p) \propto \exp\left(-\frac{p^2}{2 + V_{\theta\theta}}\right)\sqrt{4p^2 + V_{\theta\theta}(2 + V_{\theta\theta})}. \tag{47}$$

Obviously, the value of $P_\Pi(p)$ depends on the result of measurement p and different p will correspond to different resulting mechanical states. In order to simplify calculation, we choose $p = 0$ and other choice of p is also acceptable. This can be achieved by using a narrow acceptance window around $p = 0$ to perform postselection measurement to make the outcome of homodyne measurement around 0, in which case the success rate goes down but all mechanical states are created identically. Finally,

the resulting mechanical state is

$$W(\theta_M, L_M) \propto \exp\left[-\frac{1}{2}(1+V_{LL}^{-1})\theta_M^2 - \frac{1}{2}(1+V_{\theta\theta})^{-1}L_M^2\right] \times \left[(1+V_{\theta\theta})\theta_M^2 + (1+V_{\theta\theta})^{-1}L_M^2 - 1\right]. \tag{48}$$

It is obvious that when $V_{LL} \gg 1$, Wigner function $W(\theta_M, L_M)$ will near the Wigner function of squeezed single-phonon state and when $V_{LL} \to \infty$ and $V_{\theta\theta} \to 0$, $W(\theta_M, L_M)$ will near the Wigner function of single-phonon state.

C. Schrödinger catlike state

Compared with the macroscopic mechanical cat states, which are difficult to realize in experiments, the technologies of preparing optical cat state are much more mature [73–75]. Here we use the generalized photon subtraction method [71] to prepare optical cat state and the corresponding process is discussed first, see Fig. 5(a).

In the generalized photon subtracted method, the original optical input state are two unentangled squeezed states with squeezing parameters r_1 and r_2. The corresponding Wigner function of input state is

$$W_{\rm lin}(x_{1L}, p_{1L}, x_{2L}, p_{2L}) \propto W_{r_1}(x_{1L}, p_{1L}) W_{r_2}(x_{2L}, p_{2L}), \tag{49}$$

where

$$W_r(x_L, p_L) \propto \exp\left[-\frac{x_L^2}{2\exp(2r)} - \frac{p_L^2}{2\exp(-2r)}\right] \tag{50}$$

is the Wigner function of squeezed state.

Then an asymmetric beam splitter with transmittance $T_{\rm tap}$ is utilized to exchange the quantum states of the two squeezed states. If we define $\mathbf{r}_L = (x_{1L}, p_{1L}, x_{2L}, p_{2L})$, after going through the beam splitter, the resulting optical quadratures will be

$$\mathbf{r}_L \to M_L \mathbf{r}_L, \tag{51}$$

where M_L

$$M_L = \begin{pmatrix} \sqrt{T_{\rm tap}} & 0 & \sqrt{1-T_{\rm tap}} & 0 \\ 0 & \sqrt{T_{\rm tap}} & 0 & \sqrt{1-T_{\rm tap}} \\ -\sqrt{1-T_{\rm tap}} & 0 & \sqrt{T_{\rm tap}} & 0 \\ 0 & -\sqrt{1-T_{\rm tap}} & 0 & \sqrt{T_{\rm tap}} \end{pmatrix}, \tag{52}$$

is the transmission matrix of the beam splitter. According to the time-evolution formalism of Wigner function (40), the corresponding optical Wigner function $W_{L\rm tap}$ is

$$W_{L\rm tap}(x_{1L}, p_{1L}, x_{2L}, p_{2L}) \propto W_{\rm lin}(M_L^{-1} r_L). \tag{53}$$

By using a photon-number-resolved detector to measure the output photon number of the squeezed light r_2, the quantum state of the output photon on port r_2 will be projected into a catlike state

$$W_{\rm mcat}(x_{1L}, p_{1L}) \propto \int dx_{2L} dp_{2L} W_{L\rm tap}(x_{1L}, p_{1L}, x_{2L}, p_{2L}) \times W_m(x_{L2}, p_{L2}), \tag{54}$$

where $W_m(x_{L2}, p_{L2})$ is the m photons' Wigner measurement function (see Appendix B). Following these processes, we can prepare optical catlike states successfully.

By means of the optomechanical interaction (37), our torsional oscillator can be easily prepared into Schrödinger

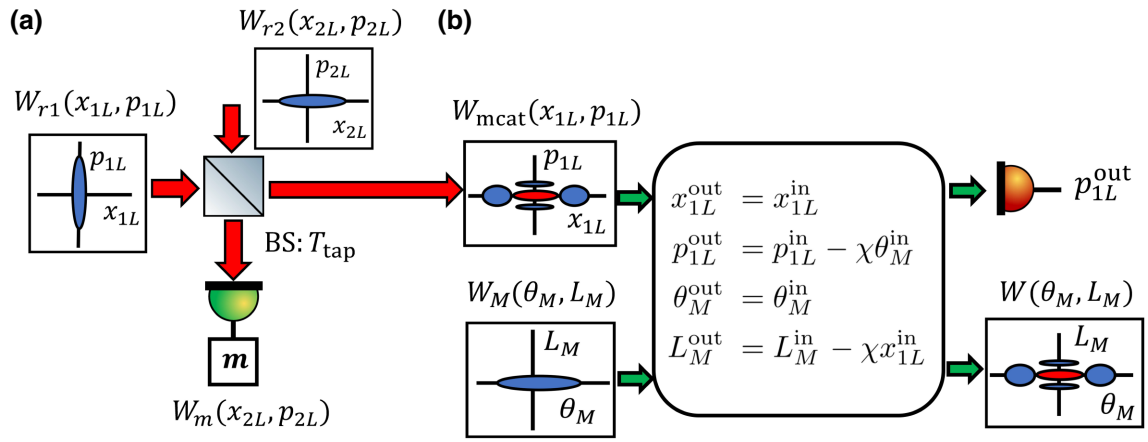

FIG. 5. (a) The preparing process of the optical cat state with Wigner function $W_{\rm mcat}(x_{1L}, p_{1L})$. BS is a beam splitter with transmittance $T_{\rm tap}$, m represents the photon number resolving detection with m photons detected and $W_m(x_{2L}, p_{2L})$ is the corresponding Wigner function. (b) State transformation and preparing process of the resulting mechanical catlike state with Wigner function $W(\theta_M, L_M)$. $p_{1L}^{\rm out}$ represents the homodyne detection on the output optical quadrature $p_{1L}^{\rm out}$.

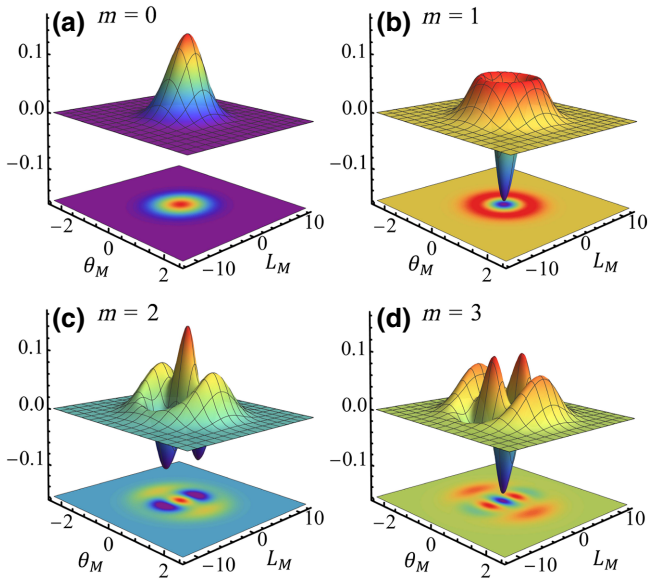

FIG. 6. The Wigner functions of the torsional oscillator prepared in Schrödinger catlike states with θ_M quadrature squeezed. In our numerical calculation, we choose $\chi = 1$, the squeezing parameters $r_1 = -r_2 = 1.15$ (i.e., 10 dB of squeezing), $T_{\rm tap} = (e^{2r_1} - 1)/(e^{2r_1} - e^{-2r_1}) \approx 0.909$ [71] and the environment temperature $T = 100$ mK.

catlike state, see Fig. 5(b), and the corresponding Wigner function is

$$W(\theta_M, L_M) \propto \int dx_{1L} dp_{1L} W_{\rm mcat}(x_{1L}, p_{1L} + \chi\theta_M) \times W_M(\theta_M, L_M + \chi x_L)\delta(p_{1L} - p). \quad (55)$$

Noting that the Wigner function of the prepared torsional cat state depends on two squeezing parameters r_1, r_2, the transmittance $T_{\rm tap}$ of an asymmetric beam splitter and the subtracted photon number m. Using experimental feasible parameters $r_1 = -r_2 = 1.15$ (i.e., 10 dB of squeezing), $T_{\rm tap} = (e^{2r_1} - 1)/(e^{2r_1} - e^{-2r_1}) \approx 0.909$ [71] and also choose $p = 0$ and $\chi = 1$, the Wigner functions of the resulting mechanical states for $m = 0, 1, 2, 3$ are plotted in Fig. 6. It can be seen that when $m > 0$, the Wigner function $W(\theta_M, L_M)$ for the output state of the torsional oscillator has negative-valued interference fringes between two significantly separated components, which demonstrates the feature of Schrödinger cat state. Noting that even if our proposal is similar to Ref. [66], in our proposal we use the generalized photon subtraction method [71] to prepare optical cat state instead of the photon subtraction method [34], which is utilized in Ref. [66], thus dramatically increasing the success probability [71] of generating optical cat state.

V. EXPERIMENTAL FEASIBILITY

The decoherence of the torsional oscillator is mainly induced by the thermal noise [48]. We consider the torsional oscillator at temperature $T = 0.1$ K with the mechanical quality factor $Q_m = 10^6$ and the torsional resonance frequency $\Omega = 2\pi \times 500$ kHz that are feasible in experiments [27,44,48,53–56]. For a mechanical cat state $|\alpha\rangle \pm |-\alpha\rangle$ with the amplitude $\alpha = 1.5$, which is comparable to the $m = 2$ and $m = 3$ states in Fig. 6, the decoherence time [76] is estimated to be

$$\tau_{\rm dec}^{\rm cat} \approx [2(1 + |\alpha|^2)\bar{n}\Gamma]^{-1} \approx 11.75\ \mu{\rm s}. \quad (56)$$

For squeezed thermal state [77],

$$\tau_{\rm dec}^{\rm th} = (2\bar{n}\Gamma)^{-1} \approx 38.19\ \mu{\rm s}. \quad (57)$$

Besides, for squeezed single-phonon state, we approximate the decoherence time to be [78]

$$\tau_{\rm dec}^{\rm single} \approx (6\bar{n}\Gamma)^{-1} \approx 12.73\ \mu{\rm s}. \quad (58)$$

Compared to the torsional oscillation period $\tau_M = 2\pi/\Omega = 2\ \mu$s, we find that it is feasible to use the present torsional model to observe macroscopic quantum effects under the realistic decoherence.

According to Eq. (25), if $\theta(z) = \cos(k_t z)$ and $|\beta_1 - \beta_2| = k_t \gg L^{-1}$, the coupling constant $g \propto \delta\epsilon\theta_{\rm ZP} \propto \delta\epsilon L^{-1/2}$ (see Appendix C). In order to observe quantum effects in longer macroscopic scale, we can increase the length L from 0.1 mm to 1 cm, e.g., with a centimeter-long optical cavity on a nanofiber [40], then the coupling constant g will reduce by an order of magnitude, which can be compensated by using the optical material with a higher optical anisotropy $\delta\epsilon$ as compared with α quartz, such as TiO_2 ($\delta\epsilon \approx 1.536$) [79] and YVO_4 ($\delta\epsilon \approx 0.936$) [80] for $\lambda = 0.63\ \mu$m.

VI. SUMMARY

We theoretically propose an angular-momentum optomechanical system, which is based on spin angular-momentum exchange interaction between light and a torsional oscillator. Our analysis shows that this system can be used to manipulate the torsional quantum state of a torsional oscillator and prepare Schrödinger catlike states with macroscopic length scale, thus providing a platform to explore the fundamental problems related with quantum torsional motion, such as the macroscopic decoherence, rotational friction [37,38], and so on. Furthermore, the relatively long optomechanical interaction length may significantly increase the scalability of optomechanical system, and thus provides us with a possibility to explore hybrid quantum optomechanics, e.g., to investigate nondemolition measurement of the phonon energy [81], sympathetic cooling of a mechanical oscillator [82].

ACKNOWLEDGMENTS

We thank Dr. Ralf Betzholz for helpful discussions. This work is supported by National Natural Science Foundation of China (Grants No. 11874024, No. 11690032, No. 12047525, and No. 12174138), the Open Project Program of Wuhan National Laboratory for Optoelectronics (2019WNLOKF002), and the Fundamental Research Funds for the Central Universities.

APPENDIX A: TIME EVOLUTION OF WIGNER FUNCTION

If the time evolution of all the quadratures $\mathbf{r}$ of a bosonic system can be described by a linear transformation, which means that

$$\mathbf{r}(T) = M\mathbf{r}(0), \tag{A1}$$

then the Wigner function and characteristic function of this system at time T can also be totally described by matrix M and the original density matrix $\rho(0)$. In order to connect the Wigner function $W(\mathbf{r}, T)$ at time T with the Wigner function $W(\mathbf{r}, 0)$ at time 0, we consider the following calculation.

Firstly, we consider the time evolution of characteristic function. At time T, the displacement operator [72] is

$$\begin{aligned} D(\boldsymbol{\beta}, T) &= \exp[i\mathbf{r}(T)^T \cdot \Omega\boldsymbol{\beta}] \\ &= \exp[i[M\mathbf{r}(0)]^T \cdot \Omega\boldsymbol{\beta}] \\ &= \exp[i\beta^T\Omega^T M\mathbf{r}(0)]. \end{aligned} \tag{A2}$$

Defining a vector $\gamma = \Omega M^T\Omega\boldsymbol{\beta}$, we have the following relation:

$$\begin{aligned} \boldsymbol{\beta}^T\Omega^T M\mathbf{r}(0) &= -\boldsymbol{\beta}^T\Omega^T M\Omega\Omega^T\mathbf{r}(0) \\ &= \boldsymbol{\beta}^T\left(-\Omega^T M\Omega\right)\Omega^T\mathbf{r}(0) \\ &= \boldsymbol{\beta}^T(\Omega M\Omega)\Omega^T\mathbf{r}(0) \\ &= \gamma^T\Omega^T\mathbf{r}(0) \\ &= \mathbf{r}(0)^T \cdot \Omega\gamma. \end{aligned} \tag{A3}$$

Therefore, at time T

$$D(\boldsymbol{\beta}, T) = \exp\left[\mathbf{r}(0)^T \cdot \Omega\gamma\right] = D(\boldsymbol{\gamma}, 0). \tag{A4}$$

The corresponding characteristic function [72] is

$$\begin{aligned} \chi(\boldsymbol{\beta}, T) &= \mathrm{Tr}[\rho(T)D(\boldsymbol{\beta}, 0)] \\ &= \mathrm{Tr}[\rho(0)D(\boldsymbol{\beta}, T)] \\ &= \chi(\gamma, 0). \end{aligned} \tag{A5}$$

Secondly, we consider the time evolution of Wigner function. If we define $\Omega M^T\Omega = K$, then $\gamma = K\boldsymbol{\beta}$. At time T,

$$\begin{aligned} W(\mathbf{r}, T) &= \frac{1}{(2\pi)^{2n}}\int d^{2n}\boldsymbol{\beta}\,\chi(\boldsymbol{\beta}, T)\exp\{-i\mathbf{r}^T \cdot \Omega\boldsymbol{\beta}\} \\ &= \frac{1}{(2\pi)^{2n}}\int d^{2n}\boldsymbol{\beta}\,\chi(K\boldsymbol{\beta}, 0)\exp\{-i\mathbf{r}^T \cdot \Omega\boldsymbol{\beta}\}. \end{aligned} \tag{A6}$$

Using coordination transformation $\beta' = K\beta$, we have

$$\begin{aligned} \mathbf{r}^T \cdot \Omega\beta &= \mathbf{r}^T \cdot \Omega K^{-1}\beta' \\ &= \mathbf{r}^T \cdot (M^{-1})^T\Omega^{-1}\beta' \\ &= (M^{-1}\mathbf{r})^T \cdot \Omega\beta'. \end{aligned} \tag{A7}$$

Therefore, the Wigner function of the total system at time T is

$$\begin{aligned} W(\mathbf{r}, T) &\propto \frac{1}{(2\pi)^{2n}}\int d^{2n}\boldsymbol{\beta}'\,\chi(\boldsymbol{\beta}', 0)\exp\{-i(M^{-1}\mathbf{r})^T \cdot \Omega\boldsymbol{\beta}'\} \\ &= W(M^{-1}\mathbf{r}, 0). \end{aligned} \tag{A8}$$

APPENDIX B: WIGNER MEASUREMENT FUNCTION

The positive operator-valued measure for photon-number-resolved detection with detection efficiency η is

$$\Pi = \Pi_m(\eta) = \eta^m\sum_{k=m}^{\infty}(1-\eta)^{k-m}C_m^k|k\rangle\langle k|, \tag{B1}$$

where $C_m^k = m!/k!(m-k)!$. The corresponding Wigner function [72]

$$\begin{aligned} W(X, Y) = \frac{1}{2\pi}\frac{(-1)^m\eta^m}{(2-\eta)^{1+m}}L_m\left(\frac{X^2+Y^2}{2-\eta}\right) \\ \times\exp\left\{-\frac{\eta}{2(2-\eta)}(X^2+Y^2)\right\}, \end{aligned} \tag{B2}$$

where $L_k(x)$ is a Laguerre polynomial.

APPENDIX C: g_{12MA}

Considering the normalized condition of $\mathbf{E}_1(\mathbf{x})$ and $\mathbf{E}_2(\mathbf{x})$, we can express g_{12MA} as

$$\begin{aligned} g_{12MA} &= \frac{\theta_{ZP}}{2}\left(\epsilon_{xx}-\epsilon_{yy}\right)\sqrt{\omega_1\omega_2} \\ &\times \frac{\int\left(E_{2x}E_{1y}^{*}+E_{2y}E_{1x}^{*}\right)dxdy}{\sqrt{\int \mathbf{E}_1\cdot\epsilon\mathbf{E}_1 dxdy}\cdot\sqrt{\int \mathbf{E}_2\cdot\epsilon_2\mathbf{E}_2 dxdy}} \\ &\times \frac{\int_{-L/2}^{L/2}\cos(k_t z)\cos\left(\beta_1 z\right)\cos\left(\beta_2 z\right)dz}{\sqrt{\int_{-L/2}^{L/2}\cos\left(\beta_1 z\right)^2 dz}\cdot\sqrt{\int_{-L/2}^{L/2}\cos\left(\beta_2 z\right)^2 dz}} \\ &\propto \theta_{ZP}\sqrt{\omega_1\omega_2}\left(\frac{\delta\epsilon}{L}\right)\int_{-L/2}^{L/2}\theta(z)\cos\left(\beta_1 z\right)\cos\left(\beta_2 z\right)dz. \end{aligned} \tag{C1}$$

In the last step, we use the approximation that $\int_{-L/2}^{L/2}\cos(\beta_1 z)^2 dz \approx \int_{-L/2}^{L/2}\cos(\beta_2 z)^2 dz \approx L/2$.

Furthermore, if $\theta(z)\propto\cos(k_t z)$, then g_{12MA} will be

$$\begin{aligned} g_{12MA} &\propto \frac{1}{L}\int_{-L/2}^{L/2}\cos(k_t z)\cos\left(\beta_1 z\right)\cos\left(\beta_2 z\right)dz \\ &= -\frac{\sin\left(\frac{1}{2}L\left(-\beta_1-\beta_2+k_t\right)\right)}{2L(\beta_1+\beta_2-k_t)} \\ &\quad+\frac{\sin\left(\frac{1}{2}L\left(\beta_1-\beta_2+k_t\right)\right)}{2L(\beta_1-\beta_2+k_t)} \\ &\quad+\frac{\sin\left(\frac{1}{2}L\left(-\beta_1+\beta_2+k_t\right)\right)}{2L(-\beta_1+\beta_2+k_t)} \\ &\quad+\frac{\sin\left(\frac{1}{2}L\left(\beta_1+\beta_2+k_t\right)\right)}{2L(\beta_1+\beta_2+k_t)}. \end{aligned} \tag{C2}$$

In this system, $\beta_1\sim 2\pi/\lambda$ and $\beta_2\sim 2\pi/\lambda$ where λ is the wavelength of the electromagnetic field. If $L\geq 0.1$ mm, $\beta_1 L\gg 1$ and $\beta_2 L\gg 1$. When $\beta_1-\beta_2=k_t\gg L^{-1}$, $\sin\left(\frac{1}{2}L\left(\beta_1-\beta_2+k_t\right)\right)/(\beta_1-\beta_2+k_t)L=\sin(k_t L)/2k_t L\ll 1$ and $\sin\left(\frac{1}{2}L\left(\beta_1-\beta_2-k_t\right)\right)/2(\beta_1-\beta_2-k_t)L=1/4$. Noting that $\theta_{ZP}=\sqrt{\hbar/(2I_{eff}\Omega)}\propto L^{-1/2}$, we have $g\approx g_{12MA}\propto\delta\epsilon\theta_{ZP}\propto\delta\epsilon L^{-1/2}$.

[1] E. Gavartin, P. Verlot, and T. J. Kippenberg, A hybrid on-chip optomechanical transducer for ultrasensitive force measurements, Nat. Nanotechnol. **7**, 509 (2012).

[2] G. Anetsberger, E. Gavartin, O. Arcizet, Q. P. Unterreithmeier, E. M. Weig, M. L. Gorodetsky, J. P. Kotthaus, and T. J. Kippenberg, Measuring nanomechanical motion with an imprecision below the standard quantum limit, Phys. Rev. A **82**, 061804 (2010).

[3] S. Basiri-Esfahani, A. Armin, S. Forstner, and W. P. Bowen, Precision ultrasound sensing on a chip, Nat. Commun. **10**, 132 (2019).

[4] K. Hammerer, M. Aspelmeyer, E. S. Polzik, and P. Zoller, Establishing Einstein-Poldosky-Rosen Channels between Nanomechanics and Atomic Ensembles, Phys. Rev. Lett. **102**, 020501 (2009).

[5] K. Stannigel, P. Rabl, A. S. Sørensen, P. Zoller, and M. D. Lukin, Optomechanical Transducers for Long-Distance Quantum Communication, Phys. Rev. Lett. **105**, 220501 (2010).

[6] M. Forsch, R. Stockill, A. Wallucks, I. Marinković, C. Gärtner, R. A. Norte, F. van Otten, A. Fiore, K. Srinivasan, and S. Gröblacher, Microwave-to-optics conversion using a mechanical oscillator in its quantum ground state, Nat. Phys. **16**, 69 (2020).

[7] J. Chen, M. Rossi, D. Mason, and A. Schliesser, Entanglement of propagating optical modes via a mechanical interface, Nat. Commun. **11**, 943 (2020).

[8] J. Chan, T. P. M. Alegre, A. H. Safavi-Naeini, J. T. Hill, A. Krause, S. Gröblacher, M. Aspelmeyer, and O. Painter, Laser cooling of a nanomechanical oscillator into its quantum ground state, Nature **478**, 89 (2011).

[9] T. P. Purdy, P.-L. Yu, R. W. Peterson, N. S. Kampel, and C. A. Regal, Strong optomechanical squeezing of light, Phys. Rev. X **3**, 031012 (2013).

[10] N. Aggarwal, T. J. Cullen, J. Cripe, G. D. Cole, R. Lanza, A. Libson, D. Follman, P. Heu, T. Corbitt, and N. Mavalvala, Room-temperature optomechanical squeezing, Nat. Phys. **16**, 784 (2020).

[11] P. Vezio, A. Chowdhury, M. Bonaldi, A. Borrielli, F. Marino, B. Morana, G. A. Prodi, P. M. Sarro, E. Serra, and F. Marin, Quantum motion of a squeezed mechanical oscillator attained via an optomechanical experiment, Phys. Rev. A **102**, 053505 (2020).

[12] A. Chowdhury, P. Vezio, M. Bonaldi, A. Borrielli, F. Marino, B. Morana, G. A. Prodi, P. M. Sarro, E. Serra, and F. Marin, Quantum Signature of a Squeezed Mechanical Oscillator, Phys. Rev. Lett. **124**, 023601 (2020).

[13] R. A. Thomas, M. Parniak, C. Østfeldt, C. B. Møller, C. Bærentsen, Y. Tsaturyan, A. Schliesser, J. Appel, E. Zeuthen, and E. S. Polzik, Entanglement between distant macroscopic mechanical and spin systems, Nat. Phys. **17**, 228 (2021).

[14] S. Kotler, G. A. Peterson, E. Shojaee, F. Lecocq, K. Cicak, A. Kwiatkowski, S. Geller, S. Glancy, E. Knill, R. W. Simmonds, J. Aumentado, and J. D. Teufel, Direct observation of deterministic macroscopic entanglement, Science **372**, 622 (2021).

[15] R. Riedinger, A. Wallucks, I. Marinković, C. Löschnauer, M. Aspelmeyer, S. Hong, and S. Gröblacher, Remote quantum entanglement between two micromechanical oscillators, Nature **556**, 473 (2018).

[16] V. Garcés-Chávez, K. Volke-Sepulveda, S. Chávez-Cerda, W. Sibbett, and K. Dholakia, Transfer of orbital angular momentum to an optically trapped low-index particle, Phys. Rev. A **66**, 063402 (2002).

[17] M. E. J. Friese, J. Enger, H. Rubinsztein-Dunlop, and N. R. Heckenberg, Optical angular-momentum transfer to trapped absorbing particles, Phys. Rev. A **54**, 1593 (1996).

[18] H. Adachi, S. Akahoshi, and K. Miyakawa, Orbital motion of spherical microparticles trapped in diffraction patterns of circularly polarized light, Phys. Rev. A **75**, 063409 (2007).

[19] M. E. J. Friese, T. A. Nieminen, N. R. Heckenberg, and H. Rubinsztein-Dunlop, Optical alignment and spinning of laser-trapped microscopic particles, Nature **394**, 348 (1998).

[20] L. Paterson, M. P. MacDonald, J. Arlt, W. Sibbett, P. E. Bryant, and K. Dholakia, Controlled rotation of optically trapped microscopic particles, Science **292**, 912 (2001).

[21] D. Oueand and M. Matsuo, Twisting optomechanical cavity (2019), ArXiv:1912.06772.

[22] M. Bhattacharyaand and P. Meystre, Using a Laguerre-Gaussian Beam to Trap and Cool the Rotational Motion of a Mirror, Phys. Rev. Lett. **99**, 153603 (2007).

[23] T. M. Hoang, Y. Ma, J. Ahn, J. Bang, F. Robicheaux, Z.-Q. Yin, and T. Li, Torsional Optomechanics of a Levitated Nonspherical Nanoparticle, Phys. Rev. Lett. **117**, 123604 (2016).

[24] R. Reimann, M. Doderer, E. Hebestreit, R. Diehl, M. Frimmer, D. Windey, F. Tebbenjohanns, and L. Novotny, Ghz Rotation of an Optically Trapped Nanoparticle in Vacuum, Phys. Rev. Lett. **121**, 033602 (2018).

[25] J. Ahn, Z. Xu, J. Bang, P. Ju, X. Gao, and T. Li, Ultrasensitive torque detection with an optically levitated nanorotor, Nat. Nanotechnol. **15**, 89 (2020).

[26] E. F. Fenton, A. Khan, P. Solano, L. A. Orozco, and F. K. Fatemi, Spin-optomechanical coupling between light and a nanofiber torsional mode, Opt. Lett. **43**, 1534 (2018).

[27] L. He, H. Li, and M. Li, Optomechanical measurement of photon spin angular momentum and optical torque in integrated photonic devices, Sci. Adv. **2**, e1600485 (2016).

[28] Z. Xuand and T. Li, Detecting Casimir torque with an optically levitated nanorod, Phys. Rev. A **96**, 033843 (2017).

[29] D. A. T. Somersand and J. N. Munday, Rotation of a liquid crystal by the Casimir torque, Phys. Rev. A **91**, 032520 (2015).

[30] J. N. Munday, D. Iannuzzi, and F. Capasso, Quantum electrodynamical torques in the presence of brownian motion, New J. Phys. **8**, 244 (2006).

[31] A. Manjavacasand and F. J. García de Abajo, Vacuum Friction in Rotating Particles, Phys. Rev. Lett. **105**, 113601 (2010).

[32] R. Zhao, A. Manjavacas, F. J. García de Abajo, and J. B. Pendry, Rotational Quantum Friction, Phys. Rev. Lett. **109**, 123604 (2012).

[33] M. Bhattacharya, P.-L. Giscard, and P. Meystre, Entanglement of a Laguerre-Gaussian cavity mode with a rotating mirror, Phys. Rev. A **77**, 013827 (2008).

[34] M. Dakna, T. Anhut, T. Opatrný, L. Knöll, and D.-G. Welsch, Generating Schrödinger-cat-like states by means of conditional measurements on a beam splitter, Phys. Rev. A **55**, 3184 (1997).

[35] J. T. Muhonen, G. R. La Gala, R. Leijssen, and E. Verhagen, State Preparation and Tomography of a Nanomechanical Resonator with Fast Light Pulses, Phys. Rev. Lett. **123**, 113601 (2019).

[36] A. Nunnenkamp, K. Børkje, and S. M. Girvin, Single-Photon Optomechanics, Phys. Rev. Lett. **107**, 063602 (2011).

[37] C. Zhongand and F. Robicheaux, Decoherence of rotational degrees of freedom, Phys. Rev. A **94**, 052109 (2016).

[38] B. A. Stickler, B. Schrinski, and K. Hornberger, Rotational Friction and Diffusion of Quantum Rotors, Phys. Rev. Lett. **121**, 040401 (2018).

[39] T. H. Stievater, M. W. Pruessner, W. S. Rabinovich, D. Park, R. Mahon, D. A. Kozak, J. B. Boos, S. A. Holmstrom, and J. B. Khurgin, Suspended photonic waveguide devices, Appl. Opt. **54**, F164 (2015).

[40] J. Keloth, K. P. Nayak, and K. Hakuta, Fabrication of a centimeter-long cavity on a nanofiber for cavity quantum electrodynamics, Opt. Lett. **42**, 1003 (2017).

[41] Q. Qiao, J. Xia, C. Lee, and G. Zhou, Applications of photonic crystal nanobeam cavities for sensing, Micromachines **9**, 541 (2018).

[42] F. Le Kienand and K. Hakuta, Cavity-enhanced channeling of emission from an atom into a nanofiber, Phys. Rev. A **80**, 053826 (2009).

[43] F. Le Kienand and K. Hakuta, Effect of an atom on a quantum guided field in a weakly driven fiber-bragg-grating cavity, Phys. Rev. A **81**, 023812 (2010).

[44] Y.-I. Sohn, R. Miller, V. Venkataraman, and M. Lončar, Mechanical and optical nanodevices in single-crystal quartz, Appl. Phys. Lett. **111**, 263103 (2017).

[45] G. Ghosh, Dispersion-equation coefficients for the refractive index and birefringence of calcite and quartz crystals, Opt. Commun. **163**, 95 (1999).

[46] P. B. Deotare, M. W. McCutcheon, I. W. Frank, M. Khan, and M. Lončar, High quality factor photonic crystal nanobeam cavities, Appl. Phys. Lett. **94**, 121106 (2009).

[47] Q. Quanand and M. Loncar, Deterministic design of wavelength scale, ultra-high Q photonic crystal nanobeam cavities, Opt. Express **19**, 18529 (2011).

[48] C. Wuttke, G. D. Cole, and A. Rauschenbeutel, Optically active mechanical modes of tapered optical fibers, Phys. Rev. A **88**, 061801 (2013).

[49] H. E. Engan, B. Y. Kim, J. N. Blake, and H. J. Shaw, Propagation and optical interaction of guided acoustic waves in two-mode optical fibers, J. Lightwave Technol. **6**, 428 (1988).

[50] C. Wuttke, *Thermal excitations of optical nanofibers measured with a cavity*, Ph.D. thesis, Ph. D. dissertation (University of Mainz, 2014) (2014).

[51] H. Kawashimaand and K. Sunaga, Torsional vibrations of quartz crystal beams, IEEE Trans. Ultrason. Ferroelectr. Freq. Control **43**, 832 (1996).

[52] J.-i. Kushibiki, M. Ohtagawa, and I. Takanaga, Comparison of acoustic properties between natural and synthetic α-quartz crystals, J. Appl. Phys. **94**, 295 (2003).

[53] B. Kim, J. Jahng, R. M. Khan, S. Park, and E. O. Potma, Eigenmodes of a quartz tuning fork and their application to photoinduced force microscopy, Phys. Rev. B **95**, 075440 (2017).

[54] R. O. Pohl, X. Liu, and E. Thompson, Low-temperature thermal conductivity and acoustic attenuation in amorphous solids, Rev. Mod. Phys. **74**, 991 (2002).

[55] S. Galliou, J. Imbaud, M. Goryachev, R. Bourquin, and P. Abbé, Losses in high quality quartz crystal resonators at cryogenic temperatures, Appl. Phys. Lett. **98**, 091911 (2011).

[56] M. Goryachev, D. L. Creedon, E. N. Ivanov, S. Galliou, R. Bourquin, and M. E. Tobar, Extremely low-loss acoustic phonons in a quartz bulk acoustic wave resonator at millikelvin temperature, Appl. Phys. Lett. **100**, 243504 (2012).

[57] J. D. Jackson, Classical electrodynamics (1999).

[58] A. Yarivand and P. Yeh, *Optical Waves in Crystals* (New York: Jhon Wiley & Sons, Hoboken, New Jersey, 1984), Vol. 5.

[59] H. Zoubiand and K. Hammerer, Optomechanical multimode Hamiltonian for nanophotonic waveguides, Phys. Rev. A **94**, 053827 (2016).

[60] S. G. Johnson, M. Ibanescu, M. A. Skorobogatiy, O. Weisberg, J. D. Joannopoulos, and Y. Fink, Perturbation theory for Maxwell's equations with shifting material boundaries, Phys. Rev. E **65**, 066611 (2002).

[61] D. F. Nelsonand and M. Lax, Theory of the photoelastic interaction, Phys. Rev. B **3**, 2778 (1971).

[62] J. Wang, Y. Shi, and S. Fan, Non-reciprocal polarization rotation using dynamic refractive index modulation, Opt. Express **28**, 11974 (2020).

[63] J. S. Bennett, K. Khosla, L. S. Madsen, M. R. Vanner, H. Rubinsztein-Dunlop, and W. P. Bowen, A quantum optomechanical interface beyond the resolved sideband limit, New J. Phys. **18**, 053030 (2016).

[64] M. R. Vanner, J. Hofer, G. D. Cole, and M. Aspelmeyer, Cooling-by-measurement and mechanical state tomography via pulsed optomechanics, Nat. Commun. **4**, 2295 (2013).

[65] M. R. Vanner, I. Pikovski, G. D. Cole, M. S. Kim, Č. Brukner, K. Hammerer, G. J. Milburn, and M. Aspelmeyer, Pulsed quantum optomechanics, Proc. Nat. Acad. Sci. **108**, 16182 (2011).

[66] U. B. Hoff, J. Kollath-Bönig, J. S. Neergaard-Nielsen, and U. L. Andersen, Measurement-Induced Macroscopic Superposition States in Cavity Optomechanics, Phys. Rev. Lett. **117**, 143601 (2016).

[67] B. Julsgaard, J. Sherson, J. I. Cirac, J. Fiurášek, and E. S. Polzik, Experimental demonstration of quantum memory for light, Nature **432**, 482 (2004).

[68] R. Y. Teh, S. Kiesewetter, P. D. Drummond, and M. D. Reid, Creation, storage, and retrieval of an optomechanical cat state, Phys. Rev. A **98**, 063814 (2018).

[69] U. Akram, W. P. Bowen, and G. J. Milburn, Entangled mechanical cat states via conditional single photon optomechanics, New J. Phys. **15**, 093007 (2013).

[70] D. Leibfried, E. Knill, S. Seidelin, J. Britton, R. B. Blakestad, J. Chiaverini, D. B. Hume, W. M. Itano, J. D. Jost, C. Langer, R. Ozeri, R. Reichle, and D. J. Wineland, Creation of a six-atom 'Schrödinger cat' state, Nature **438**, 639 (2005).

[71] K. Takase, J.-i. Yoshikawa, W. Asavanant, M. Endo, and A. Furusawa, Generation of optical Schrödinger cat states by generalized photon subtraction, Phys. Rev. A **103**, 013710 (2021).

[72] A. Ferraro, S. Olivares, and M. G. A. Paris, Gaussian states in continuous variable quantum information, (2005), ArXiv:quantph/0503237.

[73] M. Takeoka, H. Takahashi, and M. Sasaki, Large-amplitude coherent-state superposition generated by a time-separated two-photon subtraction from a continuous-wave squeezed vacuum, Phys. Rev. A **77**, 062315 (2008).

[74] H. Takahashi, K. Wakui, S. Suzuki, M. Takeoka, K. Hayasaka, A. Furusawa, and M. Sasaki, Generation of Large-Amplitude Coherent-State Superposition via Ancilla-Assisted Photon Subtraction, Phys. Rev. Lett. **101**, 233605 (2008).

[75] L. Duan, Creating Schrödinger-cat states, Nat. Photonics **13**, 73 (2019).

[76] M. S. Kimand and V. Bužek, Schrödinger-cat states at finite temperature: Influence of a finite-temperature heat bath on quantum interferences, Phys. Rev. A **46**, 4239 (1992).

[77] A. Serafini, *Quantum Continuous Variables: a Primer of Theoretical Methods* (CRC press, Boca Raton, Florida, 2017).

[78] M. Aspelmeyer, T. J. Kippenberg, and F. Marquardt, Cavity optomechanics, Rev. Mod. Phys. **86**, 1391 (2014).

[79] J. R. DeVore, Refractive indices of rutile and sphalerite, J. Opt. Soc. Am. **41**, 416 (1951).

[80] T. S. Lomheimand and L. G. DeShazer, Optical-absorption intensities of trivalent neodymium in the uniaxial crystal yttrium orthovanadate, J. Appl. Phys. **49**, 5517 (1978).

[81] B. D'Urso, M. V. G. Dutt, S. Dhingra, and N. M. Nusran, Quantum measurements between a single spin and a torsional nanomechanical resonator, New J. Phys. **13**, 045002 (2011).

[82] A. Jöckel, A. Faber, T. Kampschulte, M. Korppi, M. T. Rakher, and P. Treutlein, Sympathetic cooling of a membrane oscillator in a hybrid mechanical–atomic system, Nat. Nanotechnol. **10**, 55 (2015).

Correction: Equation (58) and the matrix following Eq. (5) contained errors and have been fixed. Indices with MA contained errors and have been reset. The panels in Figure 2 were erroneously rearranged during the production cycle and have been restored to the original order.